

Original article

3D-QSAR and molecular docking study on bisarylmaleimide series as glycogen synthase kinase 3, cyclin dependent kinase 2 and cyclin dependent kinase 4 inhibitors: An insight into the criteria for selectivity

Nigus Dessalew^{a,*}, Prasad V. Bharatam^b^a Department of Pharmaceutical Chemistry, School of Pharmacy, Addis Ababa University, P.O. Box 1176, Addis Ababa, Ethiopia^b Department of Medicinal Chemistry, National Institute of Pharmaceutical Education and Research (NIPER), Sector-67, S.A.S. Nagar, Mohali, 160 062 Punjab, India

Received 26 October 2006; received in revised form 28 December 2006; accepted 9 January 2007

Available online 24 January 2007

Abstract

Selective glycogen synthase kinase 3 (GSK3) inhibition over cyclin dependent kinases such as cyclin dependent kinase 2 (CDK2) and cyclin dependent kinase 4 (CDK4) is an important requirement for improved therapeutic profile of GSK3 inhibitors. The concepts of selectivity and additivity fields have been employed in developing selective CoMFA models for these related kinases. Initially, sets of three individual CoMFA models were developed, using 36 compounds of bisarylmaleimide series to correlate with the GSK3, CDK2 and CDK4 inhibitory potencies. These models showed a satisfactory statistical significance: CoMFA-GSK3 (r^2_{con} , r^2_{cv} : 0.931, 0.519), CoMFA-CDK2 (0.937, 0.563), and CoMFA-CDK4 (0.892, 0.725). Three different selective CoMFA models were then developed using differences in pIC_{50} values. These three models showed a superior statistical significance: (i) CoMFA-Selective1 (r^2_{con} , r^2_{cv} : 0.969, 0.768), (ii) CoMFA-Selective 2 (0.974, 0.835) and (iii) CoMFA-Selective3 (0.963, 0.776). The selective models were found to outperform the individual models in terms of the quality of correlation and were found to be more informative in pinpointing the structural basis for the observed quantitative differences of kinase inhibition. An in-depth comparative investigation was carried out between the individual and selective models to gain an insight into the selectivity criterion. To further validate this approach, a set of new compounds were designed which show selectivity and were docked into the active site of GSK3, using FlexX based incremental construction algorithm.

© 2007 Elsevier Masson SAS. All rights reserved.

Keywords: GSK3; CoMFA; QSAR; CDK2; CDK4

1. Introduction

Protein phosphorylation and dephosphorylation are important processes in the control of protein functions. Biological phosphorylation mostly occurs on serine, threonine and tyrosine residues and is catalyzed by protein kinases whose number is over 500 in the human genome. Given the importance of protein phosphorylation as a main post-translational

mechanism used by cells to regulate enzymes and other proteins and the association of many maladies with its aberrations [1], kinases have increasingly become important targets and the hunt for kinase inhibitors has been intensified and attracted a great attention in drug discovery over the years [2–7]. Glycogen synthase kinase 3 (GSK3) was originally identified and studied for its function in the regulation of glycogen synthase [8–10], the rate limiting enzyme in glycogen biosynthesis [11]. It is a serine/threonine kinase comprising two isoforms (α and β) in mammals. These isoforms share high homology (>90%) at the catalytic domain and are expressed ubiquitously in cellular systems and have similar biochemical properties [12]. GSK3 has multiple substrates [13–14] and plays a critical

* Corresponding author.

E-mail addresses: dnigus@phar.aau.edu.et, nigusd96@yahoo.com (N. Dessalew).

role in glucose homeostasis [15], CNS function, and cancer [13], circadian rhythm, cell death, cell survival and others. Cyclin dependent kinases (CDKs), the closest evolutionary relatives of GSK3, are also involved in controlling the cell cycle, apoptosis, neurodegeneration, etc. [16–18]. Judging from the importance of phosphorylation in cellular and physiological events and the diverse substrates these kinases have, CDKs/GSK3 inhibitors have a wide spectrum of therapeutic potential among which diabetes, neurodegenerative diseases [19], bipolar disorders [20], stroke, cancer, and chronic inflammatory diseases [21], proliferation of viral infections (HIV, cytomegalovirus, and herpes virus) [22] are the major ones.

Fig. 1 shows some promising classes of GSK3 inhibitors. However, almost all of them were found to show affinity towards other kinases too. Maleimide series of inhibitors (bisarylmaleimides [23], anilinomaleimides [24], bisindolylmaleimides [25], azaindolylmaleimides [26], etc.) have been reported to show a degree of selectivity towards GSK3. Although a number of diverse classes of GSK3 inhibitors have been reported so far, the selectivity problem appears to hamper all efforts. This, at least in part, stems from the fact that these kinases have the same natural

substrate, ATP, and most of the ligands act through competition with ATP. This calls for methodologies that will tackle the non-selectivity problem in drug design.

A few molecular modeling studies have been reported on the design of GSK3 inhibitors [27–29]. Vulpetti and co-workers have described structure based approaches to improve selectivity between CDK2 and GSK-3 β [30]. They employed consensus principal component analysis (CPCA) along with binding site analysis in rationally designing novel and selective benzodipyrzole as CDK2 inhibitor. Zeng et al. reported CoMFA and CoMSIA studies on aliosine derivatives [31]. The structural features of GSK-3 β active site have been characterized using selective and non-selective ATP-mimetic inhibitors by Bertrand et al. [32] while Nigus et al. employed 3D-QSAR and docking studies to design potential GSK3 inhibitors [33]. Polychronopoulos et al. identified the structural basis for selective GSK3 inhibitions using molecular docking [34]. Polgar et al. performed molecular docking based virtual screening to discriminate known GSK-3 β inhibitors and to identify new ones [35].

Selectivity has always been a difficult problem and an important subject in drug design. Molecular modeling methods

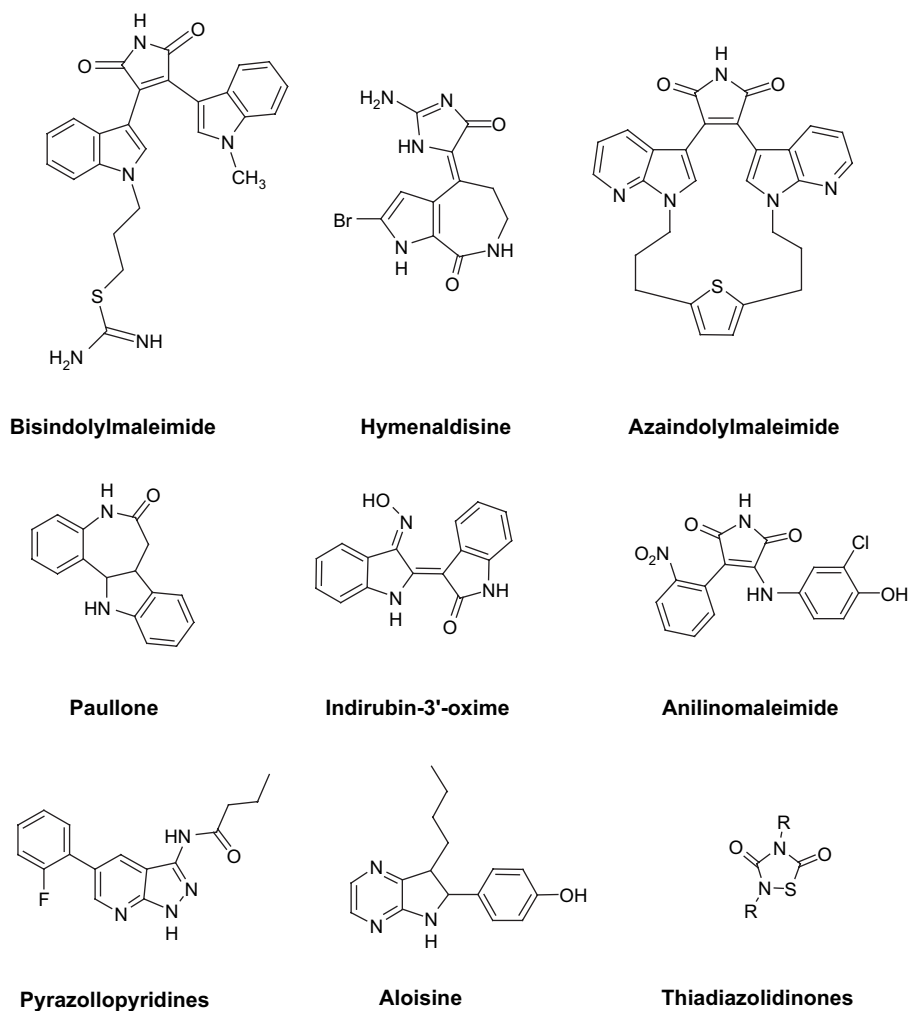


Fig. 1. GSK3 inhibitors which show a degree of selectivity towards GSK3.

can be usefully employed to tackle this issue. The current 3D-QSAR methodologies are basically designed to improve affinity. However, high affinity does not guarantee high selectivity. To address the problem of selectivity in designing a drug candidate, pairwise selectivity has been introduced by Zafirov and co-workers [36] using the differences in pK_i values between receptor subtypes as a dependent variable to develop the CoMFA models. The resulting selectivity fields provided a better quality model and indicated ways to increase the binding selectivity to either receptor. Besides other groups have also explored a concept of additivity of molecular fields in developing dual CoMFA models [37]. Both of these approaches have found their application. The validity of such considerations on molecular fields needs to be explored by further stretching to other examples on varied sets of receptor families. The work reported in this article is an attempt in that direction. CoMFA models were developed on bisarylmalimide series as GSK3, CDK2 and CDK4 inhibitors with the intention of optimizing and enhancing the selectivity towards GSK3 that will aid in designing selective molecules. The work reported here attempts to address the phenomenon of group selectivity (i.e. selectivity observed between a closely related receptor families) for the first time and thereby enhancing our understanding of the structural basis of differential activity.

2. Computational details

2.1. Dataset for analysis

The *in vitro* biological activity data reported as IC_{50} for inhibition of GSK3, CDK2 and CDK4 by the bisarylmalimide series [23] were used for the current study. In the reference paper 46 compounds were reported with their corresponding inhibitory activities expressed in IC_{50} values. Those molecules which do not have biological activity for inhibition of all the three enzymes under study in exact numerical form were excluded from the analysis. Following this 36 molecules were chosen for the current study. This was partitioned into a training set of 29 and a test set of seven compounds at random with bias given to structural diversity in both the training set and the test set so as to form the standard 4:1 training set to test set ratio for a QSAR study. As biological data are generally skewed, the reported IC_{50} values were converted into pIC_{50} .

For the individual CoMFA model generation, pIC_{50} values were obtained directly from the reported IC_{50} values. The pIC_{50} values for selective CoMFA model generation were obtained by taking the differences in pIC_{50} from the corresponding enzyme inhibitory values as follows:

$$(i) \text{ CoMFA-Sel1} = pIC_{50}(\text{GSK3}) - pIC_{50}(\text{CDK2}); \quad (1)$$

$$(ii) \text{ CoMFA-Sel2} = pIC_{50}(\text{GSK3}) - pIC_{50}(\text{CDK4}); \quad (2)$$

$$(iii) \text{ CoMFA-Sel3} = pIC_{50}(\text{CDK2}) + pIC_{50}(\text{CDK4}) - pIC_{50}(\text{GSK3}); \quad (3)$$

where the CoMFA-Sel1, CoMFA-Sel2 and CoMFA-Sel3 refer to CoMFA-Selective models 1, 2 and 3, respectively.

2.2. Molecular modeling

All molecular modeling studies were performed using the molecular modeling package SYBYL6.9 [38] installed on a Silicon Graphics Octane2 workstation. The bioactive conformation of a bisarylmalimide compound was extracted from the co-crystal complex with GSK-3 β (PDB code: 1ROE) and was used as a template for building the 3D structures of all the 36 compounds considered in this work. All the structures were further submitted to AM1 based local minimization using the MOPAC [39] package interfaced with SYBYL6.9. Partial atomic charges were computed using MOPAC applying the AM1 Hamiltonian.

2.3. Molecular alignment

One of the fundamental assumptions in 3D-QSAR studies is that a geometric parallelism should exist between the modeled structures and that of the bioactive conformation. The spatial alignment of compounds under study is thus one of the most sensitive and determining factors in obtaining a robust and meaningful model. In the present study the geometry optimized structures were aligned on the respective templates (compound **22** for GSK3 and compound **13** for CDK2 and CDK4) by the ALIGN DATABASE command in SYBYL using the maximum substructure that is common to all. Fig. 2 shows all the aligned molecules.

2.4. CoMFA interaction energies

The steric and electrostatic CoMFA potential fields were calculated at each lattice intersection of a regularly spaced grid of 2.0 Å. The grid box dimensions were determined automatically in such a way that the region boundaries were extended beyond 4 Å in each direction from the co-ordinates

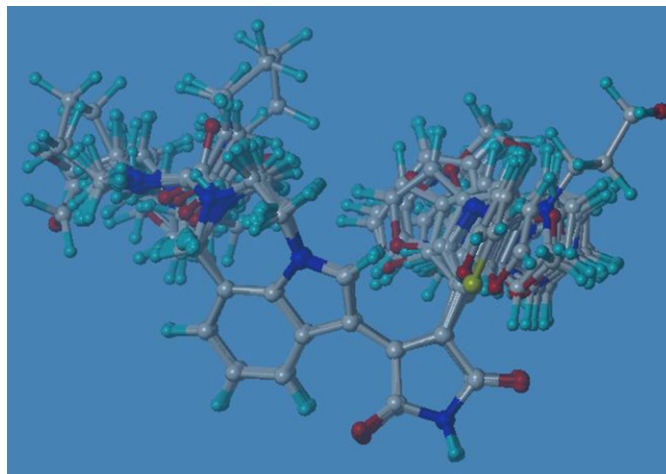


Fig. 2. Alignment of the 3D structures of the 36 molecules employed for the molecular field generation and analysis.

of each molecule. The van der Waals potential and Coulombic terms, which represent steric and electrostatic fields, respectively, were calculated using the standard Tripos force fields. A distance dependent dielectric constant of 1.00 was used. A methyl cation with +1 charge was used as a probe element to calculate steric and electrostatic fields. The steric and electrostatic contributions were truncated to +30.0 kcal/mol and electrostatic contributions were ignored at the lattice intersections with maximal steric interactions.

2.5. Partial least square (PLS) analysis

To quantify the relationship between the structural parameters (CoMFA interaction energies) and the biological activities, the PLS [40] algorithm was used. The cross-validation analysis was performed using leave-one-out (LOO) method wherein one compound is removed from the dataset and its activity is predicted using the model derived from the rest of the dataset. The cross-validated r^2 that resulted in optimum number of components and lowest standard error of prediction was taken. Equal weights for CoMFA were assigned to steric and electrostatic fields using CoMFA_STD scaling option. To speed up the analysis and reduce noise, a minimum column filtering value (σ) of 2.00 kcal/mol was used for the cross-validation. Final analysis (non-cross-validation) was performed to calculate conventional r^2 using the optimum number of components obtained from the leave-one-out cross-validation analysis. To further assess the robustness and statistical confidence of the obtained models, bootstrapping [41] analysis for 100 runs was performed.

2.6. Predictive correlation coefficient (r^2_{pred})

To further validate the derived models, biological activities of seven test set molecules were predicted using models derived from the training set. Predictive r^2 value was calculated using the formula:

$$r^2_{pred} = (SD - PRESS)/SD, \quad (4)$$

where SD is the sum of squared deviation between the biological activities of the test set molecules and the mean activity of the training set molecules and PRESS is the sum of squared deviations between the actual and predicted activities of the test set molecules.

2.7. Molecular docking

Docking of the designed molecules into the binding pocket of GSK3 was carried out using the FlexX [42] program available within SYBYL6.9 package. FlexX employs a fast algorithm for the flexible docking of small ligands into a fixed protein binding site using an incremental construction process. Standard parameters of the FlexX program as implemented in SYBYL6.9 were used during docking. To further evaluate the docking analysis, the G_score [43], PMF_score [44], D_score [45] and Chemscore [46] values were estimated using the

Cscore module of SYBYL6.9. As Cscore is a consensus scoring function, deficiency of one scoring function is expected to be addressed by another scoring function and hence the different scoring functions in it provide multiple approaches to evaluate ligand–receptor interactions.

3. Results and discussion

The 3D-QSAR CoMFA studies are carried out using the biarylmaaleimide series. Molecules that don't have bioactivity in exact numerical forms for all of the enzymes studied were removed from the analysis in order to make a comparative investigation on all of the enzymes. Initially we have been engaged in developing novel GSK3 inhibitors that will lack the problem of non-selectivity and poor pharmacokinetic properties, which appear to tarnish the so far reported inhibitors. The way to achieve high selectivity towards GSK3 has been a difficulty given the diverse substrates this enzyme has and the common mechanism it shares with other enzyme receptors. With this in mind we developed selective models in the anticipation of getting a QSAR model that would account for the bias in the biological activity seen in this series and to capitalize upon the insight from the same to design ligands with pronounced selectivity and inhibitory potency. Despite the ambiguity of the drug–receptor interaction in general and the vagueness of the GSK3 subtype used in the assay, statistically robust models were obtained both for the conventional or individual and selective models.

The CoMFA PLS analysis is summarized in Table 1. Taking r^2_{cv} , a measure goodness of prediction of a QSAR model, the conventional r^2 , which indicates goodness of fit, and other statistical parameters good models were obtained from the study. Even an important observation one can make from the study is the quality of the selective models in comparison with the individual models. This is clearly seen in the statistical parameters of CoMFA: the r^2_{cv} raised from 0.519 for GSK3, 0.563 for CDK2 and 0.725 for CDK4 to 0.768 for selective model 1, 0.835 for selective model 2, and 0.776 for selective model 3. Selective model 1 was obtained by deducting the pIC_{50} values of CDK2 from the corresponding pIC_{50} values of GSK3, while that of selective model 2 was obtained by subtracting the pIC_{50} s of CDK4 from the corresponding GSK3 pIC_{50} values. Selective model 3, on the other hand, was obtained first by adding the pIC_{50} values of both CDKs and deducting the corresponding pIC_{50} of GSK3 from the aggregate. The values thus obtained were used as a dependent variable while taking the CoMFA field values as independent variables. As such model 3 does incorporate the concepts of both selectivity and additivity of molecular fields. The conventional correlation coefficient which is used as a measure of explanatory power of the model also raised from 0.931, 0.937 and 0.892 to the corresponding 0.969, 0.974 and 0.963. The more this value is close to one implies a better quality model, the higher values obtained for the selectivity model does indicate improvement for the selective models over the individual models. To support the statistical validity of each model, bootstrapping analyses were carried out for 100 runs. In all of the cases

Table 1
Statistical parameters obtained for the different CoMFA models

QSAR parameter	Individual models			Selective models		
	CoMFA-GSK3	CoMFA-CDK2	CoMFA-CDK4	CoMFA-Sel1	CoMFA-Sel2	CoMFA-Sel3
r_{cv}^2	0.519	0.563	0.725	0.768	0.835	0.776
N	5	4	3	4	4	4
SEE	0.211	0.276	0.265	0.183	0.175	0.345
r^2	0.931	0.937	0.892	0.969	0.974	0.963
r_{pred}^2	0.787	0.856	0.919	0.854	0.853	0.908
r_{bs}^2	0.967	0.949	0.899	0.978	0.985	0.973
PRESS	1.027	1.987	1.754	0.807	0.734	2.863
F -test value	62.15	89.40	68.63	186.72	225.67	157.52
<i>Fraction of field contribution</i>						
Steric	0.522	0.565	0.557	0.563	0.605	0.536
Electrostatic	0.478	0.435	0.443	0.437	0.395	0.464

r_{cv}^2 = Cross-validated correlation coefficient; N = optimum number of components as determined by the PLS leave-one-out cross-validation study; SEE = standard error of estimate; r^2 = conventional correlation coefficient; r_{pred}^2 = predictive correlation coefficient; r_{bs}^2 = correlation coefficient after 100 runs of bootstrapping; PRESS = predictive residual sum of squares for the training set.

higher values of r_{bs}^2 were obtained which signify the robustness of the models developed. Interestingly, comparing the r_{bs}^2 values for the individual and selective models one observes once again a further improvement in favor of the selective models as compared to the individual models in the study. A further improvement on the quality of the selective models was seen from the F_{value} , which stands for the level of confidence. In the CoMFA study, the selective models provide higher values and hence higher statistical confidence. On average, the standard error of estimate was also better for the selectivity fields. These findings are in keeping with what is reported earlier [28] on pairwise selectivity (selectivity between receptor subtypes) where models from selectivity fields were found to provide a better correlation than individual models. Taking these all into account, we found that the quality of model obtained for selective models is superior as compared to the individual models. Apart from these, the range on logarithmic scale of the inhibitory activities for the selective models was found to be wider than the individual models. This is an advantage for a QSAR modeling.

The structures and actual versus predicted activities are shown in Table 2 for individual models and in Table 3 for selective models. The plots of actual and predicted activities for all the models are shown in Fig. 3. Even from the graphical display it is evident that more points lie either on the best fit line or are very close to it than for the individual models. This adds to the superiority of the selective models in contrast to individual models.

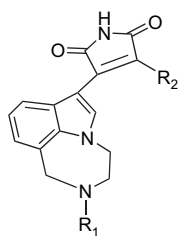
3.1. Contour analysis

The QSAR produced by a CoMFA model is usefully portrayed as a three-dimensional coefficient contour map [47]. In general, the contour maps surround all lattice points where the QSAR is found to strongly associate changes in the molecular field values (which actually stand for structural changes) with changes in binding affinity or any other measure of biological property. More specifically, the polyhedra surround

lattice points where the scalar products of the associated QSAR coefficient and the standard deviation of all values in the corresponding column of the data matrix are higher or lower than a user-specified value. In SYBYL setting, steric interactions are represented by green and yellow colored contours while electrostatic interactions are displayed as red and blue contours. Green contours stand for points where sterically bulkier groups are preferred to increase the biological activity whereas the yellow contours are used to underscore the points where bulkier groups could lower the biological property. The electrostatic red plots show where the presence of a negative charge is expected to enhance the activity whereas the blue contours indicate where introducing or keeping positive charges are expected to better the observed activity.

As can be seen from the CoMFA contours shown in Fig. 4a for GSK3 inhibition, there is a big green polyhedron incorporated on the piperidine substituent. This shows the favorability of putting or introducing bulky groups around that region so as to improve the inhibitory potency. And indeed this does explain the better activity of compounds **9**, **10**, **11**, **12**, **13**, and **14** than the corresponding compounds **1**, **2**, **3**, and **4**. This stems from the fact that the more active compounds (**9**–**14**) contain a bulky substituent that corresponding compounds **1**–**4** lack in the sterically preferred region. In addition the apparent low activity of compounds **15** in comparison with compounds **16**, **17**, **18**, **19**, and **20**, which differ only in the same green region further, proves the importance of steric preference in that area for higher activity. Moreover, the diminished GSK3 inhibitory activities of compound **31** as compared to compounds **27** and **28**, compound **32** in contrast to compound **26**, compound **36** compared to compound **30** once again adds to the need to have a bulky group at the green plot surrounding the piperidine ring for an enhanced inhibition. Apart from this there is a relatively big yellow polyhedron surrounding the pyridine ring that is fused to the imidazole moiety. This is an indication that the presence of bulky groups will be unwellcome for the inhibition of the kinase activity whereas reduction of bulkiness will be expected to improve the activity.

Table 2
Actual versus predicted pIC₅₀ from the individual CoMFA models



Compound	R ₁	R ₂	CoMFA-GSK3			CoMFA-CDK2			CoMFA-CDK4		
			Actual pIC ₅₀	Predicted		Actual pIC ₅₀	Predicted		Actual pIC ₅₀	Predicted	
				pIC ₅₀	Residual		pIC ₅₀	Residual		pIC ₅₀	Residual
1	H		8.469	8.37	0.099	7.991	8.147	−0.156	7.77	8.074	−0.304
2	H		7.387	7.401	−0.014	6.688	6.896	−0.208	7.387	7.22	0.167
3	H		8.481	8.618	−0.137	7.481	7.926	−0.445	7.636	7.398	0.238
4	H		7.886	7.801	0.085	7.041	7.296	−0.255	7.585	7.609	−0.024
5	H		7.347	7.297	0.050	7.046	6.902	0.144	7.347	7.227	0.120
6	H		7.569	7.398	0.171	5.945	5.828	0.117	6.313	6.411	−0.098
7	H		7.481	7.774	−0.293	6.44	6.845	−0.405	7.481	7.492	−0.011
8			8.824	8.834	−0.010	7.979	7.665	0.314	7.426	7.344	0.082
9			8.959	9.091	−0.132	7.754	7.91	−0.156	7.072	7.356	−0.284
10			7.721	7.635	0.086	7.119	6.799	0.320	6.876	6.958	−0.082
11			8.569	8.551	0.018	7.171	7.197	−0.026	7.025	7.121	−0.096

(continued on next page)

Table 2 (continued)

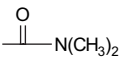
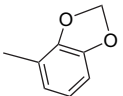
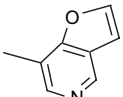
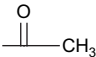
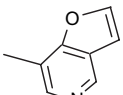
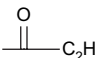
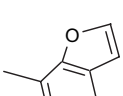

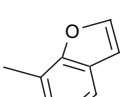
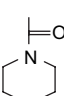
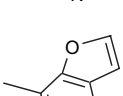
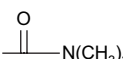
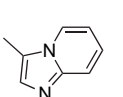

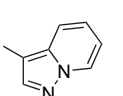
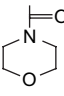
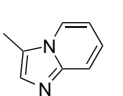
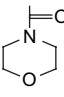
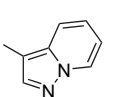
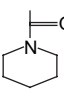
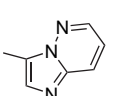

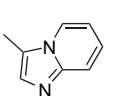
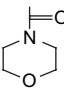
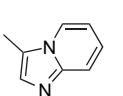
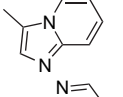
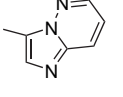
Compound	R ₁	R ₂	CoMFA-GSK3			CoMFA-CDK2			CoMFA-CDK4		
			Actual pIC ₅₀	Predicted pIC ₅₀	Residual	Actual pIC ₅₀	Predicted pIC ₅₀	Residual	Actual pIC ₅₀	Predicted pIC ₅₀	Residual
12			8.495	8.812	−0.317	6.352	6.728	−0.376	6.545	6.596	−0.051
13	H		8.495	8.439	0.056	8.194	8.055	0.139	7.717	7.526	0.191
14			9.046	8.987	0.059	8.092	7.942	0.150	7.268	7.118	0.150
15			9.00	9.122	−0.122	7.886	7.932	−0.046	7.009	7.008	0.001
16			8.921	8.945	−0.024	7.807	7.818	−0.011	6.872	6.996	−0.124
17			8.678	8.557	0.121	7.447	7.555	−0.108	6.714	6.728	−0.014
18			8.796	8.597	0.199	5.687	5.463	0.224	5.838	5.529	0.309
19			8.328	8.413	−0.085	5.657	5.737	−0.080	5.76	5.666	0.094
20			8.886	8.917	−0.031	5.49	5.594	−0.104	5.769	5.637	0.132
21			8.886	8.787	0.099	5.518	5.518	0.000	5.607	5.846	−0.239
22			9.135	9.151	−0.016	6.363	6.137	0.226	6.032	6.065	−0.033
23			8.72	8.713	0.008	6.201	6.465	−0.264	6.037	6.28	−0.243
24			9.097	9.062	0.035	5.259	5.29	−0.031	5.673	5.782	−0.109
25	H		7.921	7.504	0.417	6.121	5.892	0.229	6.807	6.353	0.454
26	H		8.319	7.977	0.342	7.173	6.471	0.702	7.143	6.567	0.576

Table 2 (continued)

Compound	R ₁	R ₂	CoMFA-GSK3			CoMFA-CDK2			CoMFA-CDK4		
			Actual pIC ₅₀	Predicted pIC ₅₀	Residual	Actual pIC ₅₀	Predicted pIC ₅₀	Residual	Actual pIC ₅₀	Predicted pIC ₅₀	Residual
27	H		6.481	7.046	−0.565	5.12	5.632	−0.512	5.335	6.079	−0.744
28	H		7.222	7.134	0.088	5.253	5.122	0.131	5.943	5.851	0.092
29	H		6.921	7.105	−0.184	5.057	5.201	−0.144	5.62	5.764	−0.144
30t	H		7.57	7.85	−0.280	6.527	6.979	0.452	7.569	7.297	0.272
31t			8.6	8.656	−0.056	7.222	6.754	0.468	6.903	6.652	0.251
32t			9.1	8.918	0.182	7.416	7.834	−0.418	6.898	6.986	−0.088
33t			8.7	8.687	0.013	5.271	5.497	−0.226	5.315	5.56	−0.245
34t			8.74	8.146	0.594	5.449	5.625	−0.176	5.439	5.782	−0.343
35t			8.46	8.398	0.062	5.788	5.62	0.168	5.966	5.866	0.100
36t	H		7.52	7.64	−0.120	6.125	5.865	0.260	6.523	6.294	0.229

Note: compound number with t refers for those compounds chosen for the test set.

Furthermore, there is another small green polyhedron that lies adjacent to the sterically unfavorable yellow region. This implies the need to have a sterically superior group to improve activity. The electrostatic contour plots also show an extended blue polyhedron over the fused imidazole–pyridine system. Such a plot points that in order to improve inhibitory activity a more electropositive atoms or groups must be introduced in the neighborhood of this region. This fact explains the better activity of compounds **31** with regard to compounds **33–35**. In addition the red polyhedron seen near the carbonyl attached to the piperidine ring implies the need to have an electron-

withdrawing group near that area for a better activity. In fact this explains why compounds which contain the carbonyl attached to N are more active than those which lack this. This can come from the fact that the lone pairs of electrons of N of the piperidine ring can go into resonance interaction thereby increasing negative charge around oxygen and hence near to the red plot. Also seen are two small red polyhedrons on opposite side of the maleimide ring indicating the demand to have electron-withdrawing groups to increase the inhibition.

Fig. 4b shows the CoMFA contours for CDK4. The contours for CDK4 show two big red polyhedrons on opposite

Table 3
Actual versus predicted pIC₅₀ values from the selective CoMFA models

Compound	CoMFA-Sel1 ^a			CoMFA-Sel2 ^a			CoMFA-Sel3 ^a		
	Actual pIC ₅₀	Predicted		Actual pIC ₅₀	Predicted		Actual pIC ₅₀	Predicted	
		pIC ₅₀	Residual		pIC ₅₀	Residual		pIC ₅₀	Residual
1	0.478	0.232	0.246	0.699	0.522	0.177	7.292	7.793	−0.501
2	0.699	0.909	−0.210	0.000	0.529	−0.529	6.686	6.214	0.472
3	1.000	1.152	−0.152	0.845	0.888	−0.043	6.636	6.495	0.141
4	0.845	0.538	0.307	0.301	0.124	0.177	6.74	7.073	−0.333
5	0.301	0.507	−0.206	0.000	−0.056	0.056	7.046	6.815	0.231
6	1.624	1.672	−0.048	1.256	1.148	0.108	4.689	4.664	0.025
7	1.041	1.067	−0.026	0.000	0.281	−0.281	6.44	6.412	0.028
8	0.845	1.035	−0.190	1.398	1.529	−0.131	6.581	6.229	0.352
9	1.205	1.018	0.187	1.887	1.797	0.090	5.867	6.218	−0.351
10	0.602	0.510	0.092	0.845	0.744	0.101	6.274	6.252	0.022
11	1.398	1.234	0.164	1.544	1.434	0.110	5.627	5.906	−0.279
12	2.143	2.053	0.090	1.950	1.962	−0.012	4.402	4.691	−0.289
13	0.301	0.599	−0.298	0.778	0.770	0.008	7.416	6.971	0.445
14	0.954	0.978	−0.024	1.778	1.775	0.003	6.314	6.208	0.106
15	1.114	1.292	−0.178	1.991	2.181	−0.190	5.895	5.68	0.215
16	1.114	1.232	−0.118	2.049	1.822	0.227	5.758	5.616	0.142
17	1.231	1.056	0.175	1.964	1.861	0.103	5.483	5.717	−0.234
18	3.109	3.207	−0.098	2.958	3.018	−0.060	2.729	2.325	0.404
19	2.671	2.596	0.075	2.568	2.652	−0.084	3.089	3.178	−0.089
20	2.946	3.155	0.209	3.117	3.328	−0.211	2.373	2.025	0.348
21	3.368	3.209	0.159	3.279	3.241	0.038	2.239	2.549	−0.310
22	2.772	2.727	0.045	3.103	3.007	0.096	3.26	3.42	−0.160
23	2.520	2.373	0.147	2.684	2.453	0.231	3.517	3.829	−0.312
24	3.838	3.794	0.044	3.424	3.453	−0.029	1.835	1.879	−0.044
25	1.800	1.472	0.328	1.114	1.055	0.059	5.007	4.925	0.082
26	1.146	1.285	−0.139	1.176	1.182	−0.006	5.997	5.411	0.586
27	1.361	1.323	0.038	1.146	1.025	0.121	3.974	4.742	−0.768
28	1.969	2.095	−0.126	1.279	1.355	−0.076	3.974	3.872	0.102
29	1.864	1.936	−0.072	1.301	1.378	−0.077	3.756	3.786	−0.030
30t	1.042	1.052	−0.010	0.000	0.655	−0.655	6.527	6.065	0.462
31t	1.380	1.603	−0.223	1.699	1.675	0.024	5.523	5.295	0.228
32t	1.681	1.361	0.320	2.199	2.075	0.124	5.217	5.177	0.040
33t	3.428	3.226	0.202	3.384	3.093	0.291	1.887	2.258	−0.371
34t	3.295	2.413	0.882	3.305	2.481	0.824	2.144	3.299	−1.155
35t	2.668	2.667	0.001	2.49	2.748	−0.258	3.298	3.041	0.257
36t	1.398	1.803	−0.405	1.000	1.473	−0.473	5.125	4.473	0.652

Note: Compound numbers with 't' indicate compounds used as a test set whereas a number without t refers to compounds used to form the training set molecules.

^a pIC₅₀ values for CoMFA-Sel1 were obtained by deducting the pIC₅₀ value of CDK2 from the corresponding values of GSK3 while that of CoMFA-Sel2 were obtained by subtracting the pIC₅₀ values of CDK2 from the corresponding values of GSK3. For CoMFA-Sel3, it was obtained first by taking the sum of CDK2 and CDK4 and then subtracting the corresponding values of GSK3 from this aggregate.

side of the maleimide ring indicating the requirement of a negatively charged group in this area to improve the activity. These were observed in the GSK3 plot almost in the same position the only difference being that their size is enlarged here. The yellow and blue polyhedra seen on the fused imidazole–pyridine system are also seen here though their sizes are reduced and there is a slight displacement of position. Seen is also one relatively small red polyhedron near the N of the fused pyridine. This indicates the need for putting an electron-withdrawing group to enhance the activity. This is in some accord with the observed fact for GSK3 inhibition and once again explains why compound **32** is more active than compounds **31**, **33**, **34**, **35**, and **36**. Also seen is a big blue polyhedron around the fused pyridine indicating the favorability of electropositive centers there. This further explains why compounds **33**, **34** and **35** are less active than compound **31**. As can be seen there is also a sterically forbidden yellow

zone extending over atoms of the pyridine ring that warns against keeping or adding bulky groups. In a sharp contrast to GSK3 a blue polyhedron is noticed in the region of carbonyl attached to the piperidine substituent. This is one of the major differences that appear to attribute to the differential activity observed. Compounds that possess carbonyl group at this region are more active as GSK3 inhibitors whereas exactly the reverse is noticed for CDK4 inhibition. Moreover, a green plot is seen near the imidazole fused to pyridine calling for sterically superior groups to improve activity.

From contour maps for CDK2 as displayed in Fig. 4c, the red polyhedron of GSK3 and the blue counterpart of CDK4 have almost disappeared at the carbonyl attached to the piperidine ring. The yellow and blue contours surrounding the fused imidazole–pyridine rings are similar with that of CDK4 contour. One notable difference of this plot from that of CDK4 is the appearance of a small blue plot on the position of the big

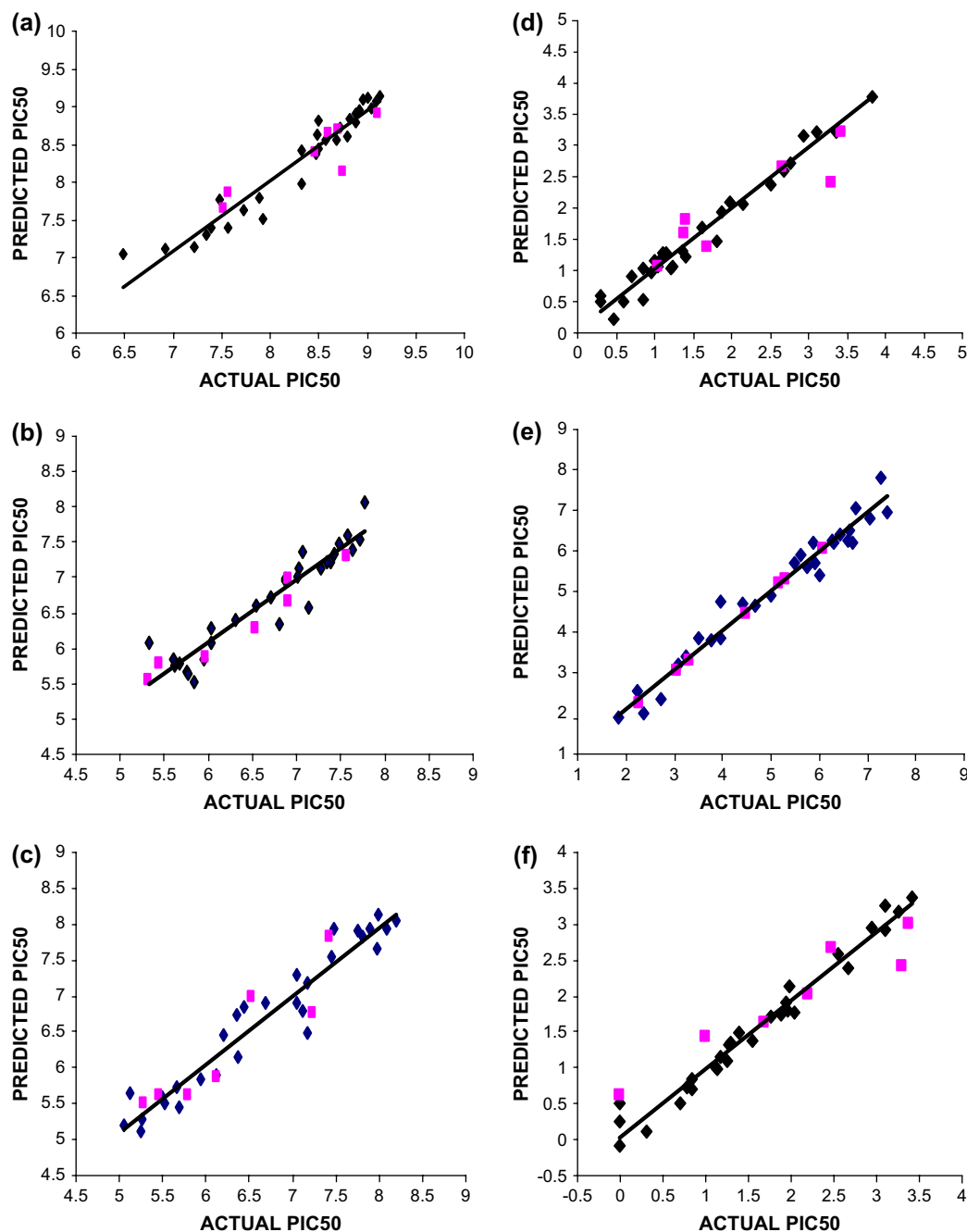


Fig. 3. Plots of actual versus predicted activities of training (shown in dark) and test set (shown in red) molecules. (a) For CoMFA-GSK3, (b) for CoMFA-CDK2, (c) for CoMFA-CDK4, (d) for CoMFA-Sel1, (e) for CoMFA-Sel2, (f) for CoMFA-Sel3. (For interpretation of the references to colour in this figure legend, the reader is referred to the web version of this article.)

blue contour seen for GSK3. In addition to the single green polyhedron of CDK4 another has appeared almost on the exact opposite of the position for CDK4. This indicates the fact that sterically superior groups are welcome here for activity betterment. Apart from this, the two red polyhedrons observed for CDK4 and GSK3 are also noticed here but their size is larger than that of GSK3 and smaller than that of CDK4 contours.

The contours for selective model 2 as displayed in Fig. 5b show a very big green map engulfing the piperidine ring. In such selectivity fields green stands for favoring GSK3 inhibition, yellow for disfavored region for GSK3 while the reverse

(green contours indicate disfavored regions and yellows imply favorable regions) holds true for CDK4 inhibition. Actually this was seen for GSK3 in the individual model but not for the separate CDK4 model. Interestingly, this is what explains the high GSK3/CDK4 activity ratio of compounds 1–6: 0.2 for compound 1, 1 for compound 2, 0.14 for compound 3, 0.28 for compound 4, 1 for compound 5, and 0.6 for compound 6 as compared to the corresponding ratio of compounds 9–14: 0.04 for compound 9, 0.01 for compound 10, 0.02 for compound 11, 0.14 for compound 12, 0.03 for compound 13 and 0.01 for compound 14. In addition a high GSK3/CDK4

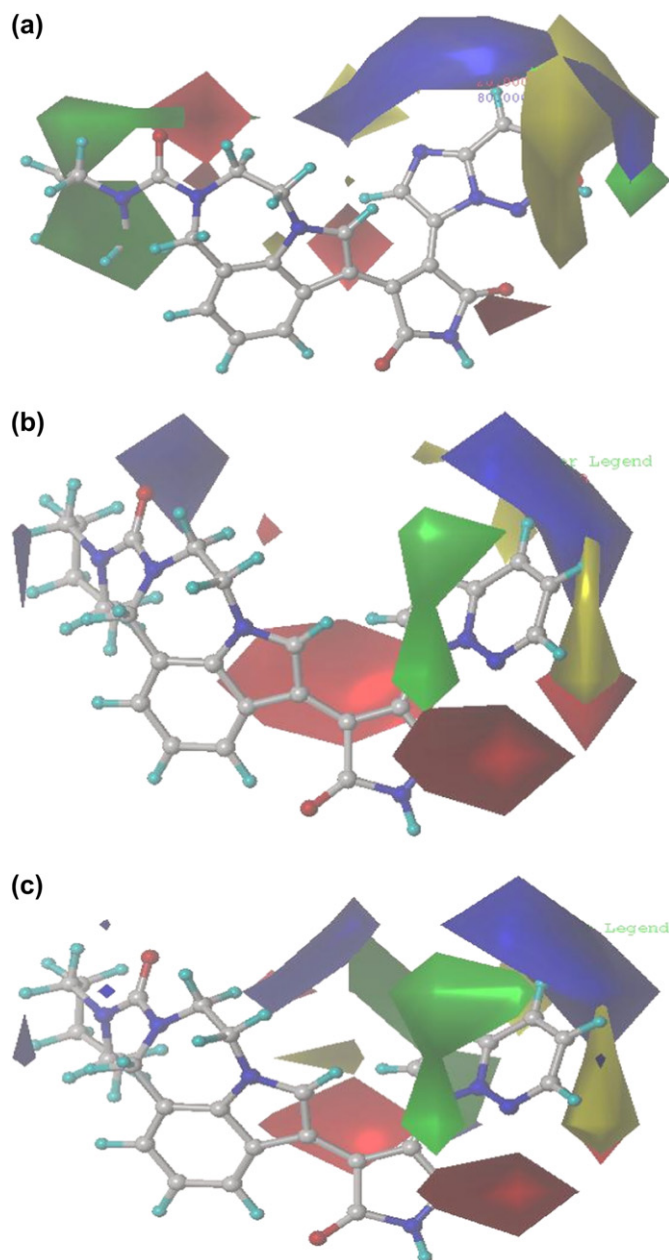


Fig. 4. CoMFA STDEVXCOEFF contour maps figure for CoMFA-GSK3 (a), CoMFA-CDK2 (b), and CoMFA-CDK4 (c). Compound **22** is displayed in all backgrounds. (For interpretation of the references to colour in this figure legend, the reader is referred to the web version of this article.)

ratio is observed for compound **15** as compared to compounds **16**, **17**, **18**, **19** and **20**. This is particularly striking as there is no such information on the separate CDK4 model. Moreover, the red polyhedron around the adjacent green plot in the region of the C=O attached to piperidine proves the favorability of an electron-withdrawing group in that region for GSK3 and the reverse for CDK4. This is what is exactly noticed from the individual models. Plus, the green contour polyhedron for CDK4 has been replaced with a yellow for this model in keeping with what is observed thus far. Such a yellow region for this model indirectly means a green plot for CDK4 inhibition. The blue contour of GSK3 is also noticed here though there is a shift

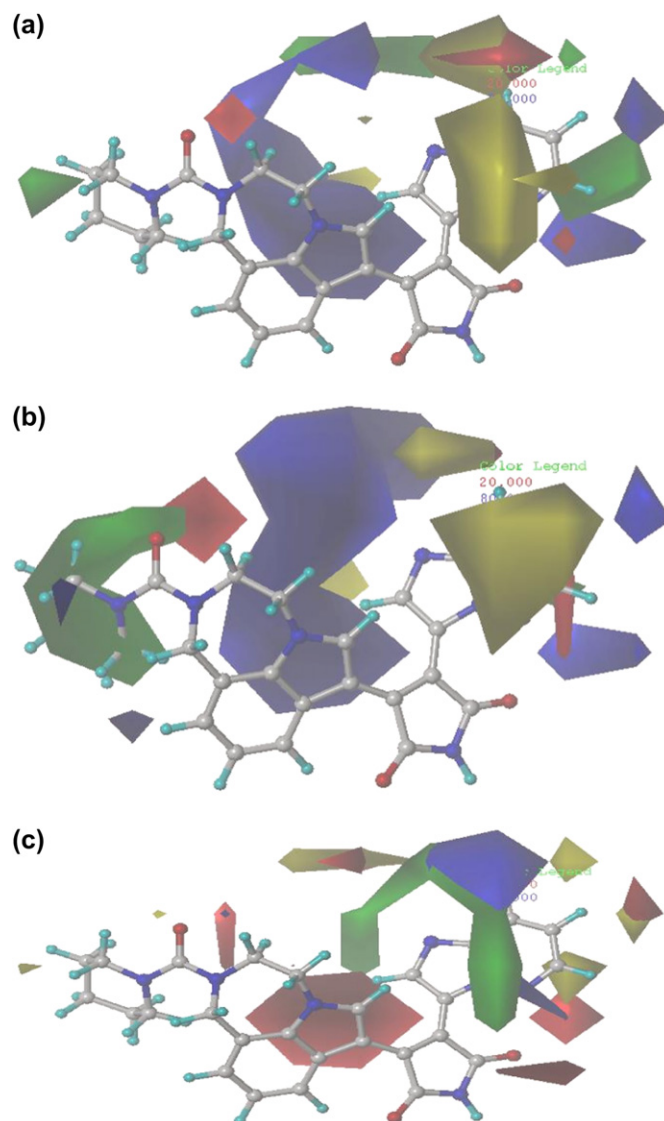


Fig. 5. CoMFA STDEVXCOEFF contour maps for CoMFA-Sel1 (a), CoMFA-Sel2 (b), and CoMFA-Sel3 (c). Compound **22** is displayed in all backgrounds. (For interpretation of the references to colour in this figure legend, the reader is referred to the web version of this article.)

in position to the right. The two red polyhedra on the opposite side of the maleimide ring have disappeared from this contour. Another red polyhedron is seen closer to the atoms of pyridine. As it is more sharp and more close to the ring it does provide a much-focused view on the factors that matter activity.

The contour map for selective model 1 displayed in Fig. 5a shows a small green plot surrounding the piperidine ring while such a plot is very large in the contours of GSK3 and selective model 2, for this model it was a small green polyhedron. This implies the importance of bulky substituent for GSK3 but such impact for CDK2 activity is apparently less in this region. From this it appears that bulky substituent is more favorable for GSK3, not preferable for CDK4 and intermediate for CDK2. As a matter of fact this is what is observed for compounds **9**, **10**, **11**, **12**, **13** and **14**. These compounds possess high GSK3 activity, low CDK4 inhibitory potency and

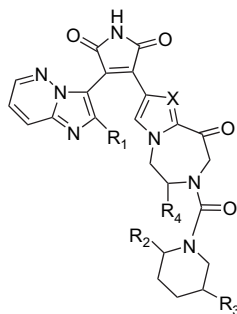
intermediate CDK2 inhibitory activity. The red polyhedron is still there near the carbonyl attached to piperidine proving its importance for GSK3 and unimportance for CDK2 inhibition. This is also revealing because of its absence in the individual CDK2 model and its requirement for GSK3 as it is observed there. Compounds that own carbonyl group are more active as GSK3 inhibitors whereas the reverse is the case for CDK2 inhibition. The big blue map is more or less the same with selective model 2 except a slight reduction in size. The other two small blue contours are also there in the same position as that of CDK4. This time a new green plot is seen between them. And the forbidden yellow contours adjacent to the pyridine ring are still present but with less volume. The contour map of the selective model 3 is shown in Fig. 5c. In this case the polyhedrons have the following meaning: green stands for favorability of increasing bulkiness to enhance both CDK2 and CDK4 inhibitions while it means the opposite for GSK3 activity: the yellow contours on the other hand imply steric preference for increasing GSK3 inhibition while reducing both CDK2 and CDK4 inhibitions. The red contours indicate where negative charges would improve both the CDKs' inhibition while the blue will reduce it and the opposite holds true for GSK3 inhibitions. As can be seen from the plot, a small yellow map is observed on opposite side of the piperidine ring which implies disfavourable region for CDK2 and CDK4 activities and favorable region for GSK3. This once again is in accord with what is observed so far both from individual models and other selective models. In addition to

this a blue plot near the N of pyridine indicates the preference of an electropositive group for both CDK2 and CDK4 and an electron-withdrawing group for GSK3. This is also what is observed from the individual models. Here it is more compact and reduced in size. This unambiguously tells where a bulky group must be kept to improve activity for GSK3 and reduce the same for both CDK2 and CDK4. The almost U-shaped green polyhedron that surrounds the imidazole ring does indicate where a steric enhancement could improve both the CDK2 and CDK4 while at the same time curtailing the GSK3 activity. The blue plot that is fused to the green region has also reduced volume than that of contours of individual CDKs and indicates where a positively charged group would enhance the CDK4 and CDK2 activities while reducing GSK3 activity. The two red polyhedra on the opposite side of the maleimide ring observed for individual CDK4 and CDK2 models have appeared here. It did not appear in the selective models 2 and 1. This further emphasizes the need to increase a negative charge around this area to improve CDK2 and CDK4 inhibitions.

From the above contour map analysis the following points clearly emerge: (I) To improve GSK3 selectivity, bulky substituents are required on piperidine ring. (II) The piperidine ring and its attached carbonyl functionality reduce the selectivity towards CDK2 and CDK4. (III) Fused tricyclic system imparts conformation rigidity. (IV) Electronegative substituents are preferred on the diazaheptane ring at the fifth position. In designing new molecules with improved selectivity towards GSK3, we followed these clues.

Table 4

Structures, predicted pIC₅₀ and docking scores of designed molecules and compound **26**



Sr. no.	Substituents					Predicted pIC ₅₀ for CoMFA			Docking scores					
	R ₁	R ₂	R ₃	R ₄	X	GSK3	CDK2	CDK4	FlexX score	G_score	PMF_score	D_score	Chemscore	Potency ^a
1	H	H	H	H	C	9.211	6.310	6.477	−27.6	−290.5	−37.8	−145.0	−33.4	1.20
2	H	Me	H	H	C	9.288	6.312	6.451	−26.7	−257.7	−55.3	−133.5	−34.7	1.42
3	H	H	H	H	C	9.510	5.965	5.288	−28.4	−308.9	−35.7	−144.0	−32.8	2.37
4	H	Me	H	H	N	9.559	6.031	6.286	−27.6	−290.3	−37.8	−145.0	−33.4	2.65
5	H	Me	H	NH ₂	N	9.673	6.063	6.293	−30.0	−307.0	−43.3	−148.3	−33.5	3.45
6	H	Me	Me	H	N	9.576	5.983	6.215	−27.7	−186.1	−62.3	−97.1	−30.5	2.76
7	H	Me	Et	H	N	9.581	5.875	6.160	−27.0	−296.1	−45.9	−152.9	−33.1	2.79
8	H	Me	Pr	H	N	9.670	5.770	6.105	−26.5	−313.8	−44.6	−161.2	−34.3	3.43
9	NH ₂	Me	ⁱ Pr	H	N	9.649	5.511	6.017	−27.2	−300.6	−49.3	−157.2	−34.0	3.27
10	NHNH ₂	Me	ⁱ Pr	H	N	9.648	5.459	6.056	−26.9	−66.9	−56.8	−108.2	−28.0	3.26
11	NH ₂	Me		H	N	9.627	5.330	5.951	−27.4	−81.6	−62.2	−117.8	−29.6	3.10
Reference						9.151	6.363	6.032	−25.8	−267.8	−20.5	−141.7	−36.5	1.00

^a Refers to the inhibitory potency for GSK3 compared to reference molecule (compound **22**) estimated as a ratio of computed IC₅₀ values.

4. Design of new molecules

As ligand based design tools, 3D-QSARs are widely employed to alter a given structural scaffold so as to come up with new molecules that have an improved biological property. Following detailed contour analyses of both the individual and selective models as discussed in the previous section several clues on the structural requirement for the observed inhibitory activities and selectivity were obtained. We have employed these clues to modify the basic skeleton to further bias the inhibition towards GSK3. Compound **22**, the most active GSK3 inhibitor of the series was used as a starting structure. Shown in Table 4 are the set of 11 designed molecules which showed improved inhibitory potency against GSK3 with respect to the reference compound **22**. Structurally, these molecules differ from the reported molecules in that the phenyl ring fused to the five- and seven-membered ring is removed. This resulted in the favorable placement of the remaining structure in the contours. This was followed by the suitable introduction of a carbonyl group on the seven-membered ring and making substitutions on the piperidine ring so as to improve bulkiness on the sterically preferred region surrounding the piperidine moiety.

All the newly designed molecules showed better selectivity according to the CoMFA predictions. However, there is a need to validate these predictions. The FlexX method of molecular docking has been employed for this purpose. The preliminary condition for validation is that these molecules should get successfully docked into the active site. Secondary condition is that the docking scores should be relatively better than the reference systems. A total of about 35 molecules were designed which showed improved IC_{50} values over the reference compound **22** and docked well. Based on the FlexX and other docking scores 11 molecules are considered as new potent ligands (Table 4). A quantitative estimate of the relative binding affinities of these ligands has been obtained using five different scoring functions: FlexX, G_score, PMF_score, D_score and Chemscore. These designed molecules indeed show better scores in comparison to the reference compound. This indicates that there is a greater chance of the newly designed molecules to be selective towards GSK3 inhibition. Table 4 also includes the relative potency of the new molecules on the basis of their calculated IC_{50} values in comparison with the best inhibitor of the series studied.

4.1. Binding mode of hit-N11 with GSK3 active site

The interaction of the best FlexX scoring hit is displayed in Fig. 6. As the display shows, the NH of Val135 is making a hydrogen bonding interaction with the carbonyl of the maleimide moiety of the hit. The NH on the maleimide moiety is also seen to make hydrogen bonding interactions with the carbonyl of Asp133. Apart from this Gln185 is also noticed to make another hydrogen bonding interaction with the carbonyl group that connects the piperidine with the azapane ring. Moreover, Arg141 is also making interactions with the amino substituents on the azapane ring via hydrogen bond interactions.

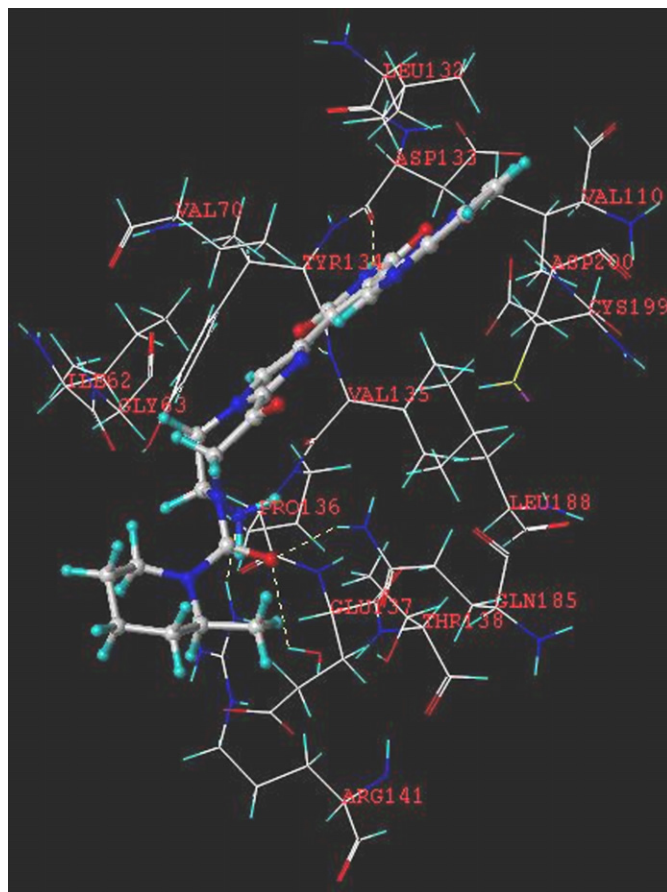


Fig. 6. Binding mode of hit-n11. Dotted lines indicate hydrogen bonding interactions.

A potential hydrophobic interaction also appears between Val70 and Ile62 of the active site and that of the azepane ring of the molecule. These amino acids are found to be important in interacting with the so far reported inhibitors of GSK3 [32].

5. Conclusions

A set of 36 compounds belonging to bisarylmalimide series have been employed to develop correlation with the biological activities against the three enzyme receptors: GSK3, CDK2 and CDK4. The validity of the correlation has been established using the PLS statistical parameters, the predictive power of the models and the contour map analysis. Selectivity fields have been developed using the difference in pIC_{50} values. Using this approach, three different selective CoMFA models were developed. The contour maps of the selective models revealed a way that could be employed to bias the inhibitory activity towards either of the receptors and helped in explaining the structural basis for the experimentally observed differences in activity.

The validity of the selective models has been checked using different approaches. First, the correlative and predictive abilities of the selective models were evaluated from the PLS statistical parameters. All of the selective models were found to

provide a better quality model as compared to the conventional individual models. Secondly, the contour analyses of the selective and individual models were used as another means of validation. Molecules that showed a good fit in the contours of the selective models were found to exhibit a better selectivity in the inhibitory potencies used to develop the selective model. As a final validation criterion, new molecules were designed using the individual and selective models by making a suitable modification to the basic skeleton in the favorable contour regions. The molecules showed a better predicted pIC_{50} values. Furthermore, docking of these molecules in the active site of GSK3 provided a good fit in terms of the FlexX and other docking scores.

As the problem of selectivity is one of the bottlenecks in contemporary drug discovery, the insight provided from this study could aid in further designing novel ligands with enhanced receptor discrimination. The analysis of contours for the individual models has provided an idea about the structural requirement for the observed biological activity for the respective kinases. The analysis of the selective models also revealed the structural needs for the observed selectivity of kinase inhibition. Taken together, this could help further design of compounds with an enhanced activity or to guide the prioritization of potential druggables for the purpose of synthesis and virtual screening of chemical databases. As the use of selectivity fields in guiding design and synthesis is just emerging to be understood, more work in this area will be required to further substantiate its application on a diverse set of receptors.

References

- [1] S. Renfrey, J. Featherstone, *Nat. Rev. Drug Discov.* 1 (2002) 175–176.
- [2] P. Cohen, *Nat. Rev. Drug Discov.* 1 (2002) 309–315.
- [3] M.E. Noble, J.A. Endicott, L.N. Johnson, *Science* 303 (2004) 1800–1805.
- [4] J.L. Adams, D. Lee, *Curr. Opin. Drug Discov. Dev.* 2 (1999) 96–109.
- [5] C. Garcia-Echeverria, P. Traxler, D.B. Evans, *Med. Res. Rev.* 20 (2000) 28–57.
- [6] R. Sridhar, O. Hanson-Painton, D.R. Cooper, *Pharm. Res.* 17 (2000) 1345–1353.
- [7] J. Dumas, *Expert Opin. Ther. Patents* 11 (2001) 405–429.
- [8] S. Frame, P. Cohen, *Biochem. J.* 359 (2001) 1–16.
- [9] B.W. Doble, J.R. Woodget, *J. Cell. Sci.* 116 (2003) 1175–1186.
- [10] R.S. Jope, G.V.W. Johnson, *Trends Biochem. Sci.* 29 (2004) 95–102.
- [11] G.I. Welsh, C.G. Proud, *Biochem. J.* 294 (1993) 625–629.
- [12] J.R. Woodget, *EMBO J.* 9 (1990) 2431–2438.
- [13] C.A. Grimes, R.S. Jope, *Prog. Neurobiol.* 65 (2001) 391–426.
- [14] H. Eldar-Finkelman, *Trends Mol. Med.* 8 (2002) 126–132.
- [15] O. Kaidanovich, H. Eldar-Finkelman, *Expert Opin. Ther. Targets* 6 (2002) 555–561.
- [16] D.O. Morgan, *Ann. Rev. Cell. Dev. Biol.* 13 (1997) 261–291.
- [17] M. Malumbres, S. Ortega, M. Barbacid, *Biol. Chem.* 381 (2000) 827–838.
- [18] R. Dhavan, L.H. Tsai, *Nature Rev. Mol. Cell Biol.* 2 (2001) 749–759.
- [19] A. Castro, A. Martinez, *Expert Opin. Ther. Patents* 10 (2000) 1519–1527.
- [20] C.J. Phiel, P.S. Klein, *Ann. Rev. Pharmacol. Toxicol.* 41 (2001) 789–813.
- [21] K.P. Hoefflich, J. Luo, E.A. Rubie, M.S. Tsao, O. Jin, J.R. Woodget, *Nature* 46 (2000) 86–90.
- [22] M. Knockaert, P. Greengard, L. Meijer, *Trends Pharmacol. Sci.* 23 (2002) 417–425.
- [23] T.A. Engler, S. Malhotra, T.P. Burkholder, J.R. Henry, D. Mendel, W.J. Porter, K. Furness, C. Diefenbacher, A. Marquart, J.K. Reel, Y. Li, J. Clayton, B. Cunningham, J. McLean, J.C. O'Toole, J. Brozinick, E. Hawkins, E. Misener, D. Briere, R.A. Brier, J.R. Wagner, R.M. Campbell, B.D. Anderson, R. Vaughn, D.B. Bennet, T.I. Meier, J.A. Cook, *Bioorg. Med. Chem. Lett.* 15 (2005) 899–903.
- [24] D.G. Smith, M. Buffet, A.E. Fenwick, D. Haigh, R.J. Iffe, M. Saunders, P.S. Brian, R. Stacey, R.W. Ward, *Bioorg. Med. Chem. Lett.* 11 (2001) 635–639.
- [25] Z. Hang-Cheng, B.W. Kimberly, Y. Hong, F.M. David, K.D. Claudia, F.A. Michael, A.G. Patricia, J.E. Annette, R.C. Bruce, W. Lori, Z.X. Jun, A.L. Richard, T.D. Keith, E. Stuart, E.M. Bruce, *Bioorg. Med. Chem. Lett.* 13 (2003) 3049–3053.
- [26] K. Gee-Hong, P. Catherine, D. Alan, S. Lan, J.O. David, S. Chandra, J.C. Peter, V.M. William, R.C. Bruce, C. Peter, W. Lori, Z. Jun, A.L. Richard, T.D. Keith, E. Stuart, A.M. Steven, J. Linda, P.B. Mary, C. Xin, *J. Med. Chem.* 46 (2003) 4021–4031.
- [27] A. Martinez, M. Alonso, A. Castro, I. Dorronsoro, J.L. Gelpi, F.J. Luque, C. Perez, F.J. Moreno, *J. Med. Chem.* 48 (2005) 7103–7112.
- [28] C. Kunick, K. Lauenroth, K. Wiekling, X. Xie, C. Schultz, R. Gussio, D. Zaharevitz, M. Leost, L. Meijer, A. Weber, F.S. Jorgensen, T. Lemcke, *J. Med. Chem.* 47 (2004) 22–36.
- [29] S.K. Singh, N. Dessalew, P.V. Bharatam, *Eur. J. Med. Chem.* 41 (2006) 1310–1319.
- [30] A. Vulpetti, P. Crivori, A. Cameron, J. Bertrand, M.G. Brasca, R. D'Alessio, P. Paverello, *J. Chem. Inf. Model.* 45 (2005) 1282–1290.
- [31] M. Zeng, Y. Jiang, B. Zhang, K. Zheng, N. Zhang, Q. Yu, *Bioorg. Med. Chem. Lett.* 15 (2005) 395–399.
- [32] J.A. Bertrand, S. Thieffine, A. Vulpetti, C. Cristiani, B. Valsasina, S. Knapp, H.M. Kalisz, M. Flocco, *J. Mol. Biol.* 333 (2003) 393–407.
- [33] N. Dessalew, D.S. Patel, P.V. Bharatam, *J. Mol. Graph. Mod.* 25 (2007) 885–895.
- [34] P. Polychronopoulos, P. Magiatis, A.L. Skaltsounis, V. Myrianthopoulos, E. Mikros, A. Tarricone, A. Musacchio, S.M. Roe, L. Pearl, M. Leost, P. Greengard, L. Meijer, *J. Med. Chem.* 47 (2004) 935–946.
- [35] T. Polgar, A. Baki, G.I. Szendrei, G.M. Keseruu, *J. Med. Chem.* 25 (2005) 7946–7959.
- [36] I. Igor, I. Baskin, G. Tikhonova, A.P. Vladimir, N.S. Zefirov, *J. Med. Chem.* 46 (2003) 4063–4069.
- [37] S. Khanna, M.E. Sobhia, P.V. Bharatam, *J. Med. Chem.* 48 (2005) 3015–3025.
- [38] SYBYL6.9, Tripos Inc., 1699 South Hanley Rd., St. Louis, MO 63144, USA.
- [39] M.J.S. Dewar, E.G. Zebisch, E.F. Healy, J.J.P. Stewart, *J. Am. Chem. Soc.* 107 (1985) 3902–3909.
- [40] S. Wold, A. Johansson, M. Cochi, in: H. Kubinyi (Ed.), *3D QSAR in Drug Design: Theory, Methods and Applications*, ESCOM, Lieden, 1993, pp. 523–550.
- [41] R.D. Cramer III, J.D. Bunce, D.E. Patterson, *Quant. Struct. Act. Relat.* 7 (1988) 18–25.
- [42] M. Rarey, B. Kramer, T. Lengauer, G. Klebe, *J. Mol. Biol.* 261 (1996) 470–489.
- [43] G. Jones, P. Willett, R.C. Glen, A.R. Leach, R. Taylor, *J. Mol. Biol.* 267 (1997) 727–748.
- [44] I. Muegge, Y.C. Martin, *J. Med. Chem.* 42 (1999) 791–804.
- [45] I.D. Kuntz, J.M. Blaney, S.J. Oatley, R. Langridge, T.E. Ferrin, *J. Mol. Biol.* 161 (1982) 269–288.
- [46] M.D. Eldridge, C.W. Murray, T.R. Auton, G.V. Paolini, R.P. Mee, *J. Comput. Aided Mol. Des.* 11 (1997) 425–445.
- [47] R.D. Cramer III, D.E. Patterson, J.D. Bunce, *J. Am. Chem. Soc.* 110 (1988) 5959–5967.